arXiv:1703.10222v1 [cs.SY] 29 Mar 2017

Plug-and-play and coordinated control for bus-connected AC islanded microgrids

Stefano Riverso * [1], Michele Tucci †[2], Juan C. Vasquez ‡ [3], Josep M. Guerrero § [3], and Giancarlo Ferrari-Trecate ¶[4]

[1] *United Technologies Research Center Ireland, 4th Floor, Penrose Business Center, Penrose Wharf, Cork, Ireland*
[2] *Dipartimento di Ingegneria Industriale e dell'Informazione, Università degli Studi di Pavia, Italy*
[3] *Institute of Energy Technology, Aalborg University, 9220 Aalborg, Denmark*
[4] *Automatic Control Laboratory, École Polytechnique Fédérale de Lausanne (EPFL), Switzerland*

Technical Report
March, 2017

Abstract

This paper presents a distributed control architecture for voltage and frequency stabilization in AC islanded microgrids. In the primary control layer, each generation unit is equipped with a local controller acting on the corresponding voltage-source converter. Following the plug-and-play design approach previously proposed by some of the authors, whenever the addition/removal of a distributed generation unit is required, feasibility of the operation is automatically checked by designing local controllers through convex optimization. The update of the voltage-control layer, when units plug -in/-out, is therefore automatized and stability of the microgrid is always preserved. Moreover, local control design is based only on the knowledge of parameters of power lines and it does not require to store a global microgrid model. In this work, we focus on bus-connected microgrid topologies and enhance the primary plug-and-play layer with local virtual impedance loops and secondary coordinated controllers ensuring bus voltage tracking and reactive power sharing. In particular, the secondary control architecture is distributed, hence mirroring the modularity of the primary control layer. We validate primary and secondary controllers by performing experiments with balanced, unbalanced and nonlinear loads, on a setup composed of three bus-connected distributed generation units. Most importantly, the stability of the microgrid after the addition/removal of distributed generation units is assessed. Overall, the experimental results show the feasibility of the proposed modular control design framework, where generation units can be added/removed on the fly, thus enabling the deployment of virtual power plants that can be resized over time.

Keywords: Distributed control, secondary control, plug-and-play design, AC islanded microgrid, voltage and frequency control.

*Electronic address: riverss@utrc.utc.com
†Electronic address: michele.tucci02@universitadipavia.it
‡Electronic address: juq@et.aau.dk
§Electronic address: joz@et.aau.dk
¶Electronic address: giancarlo.ferraritrecate@epfl.ch

1 Introduction

Islanded microGrids (ImGs) are autonomous energy systems composed of the interconnection of Distributed Generation Units (DGUs) and loads. In view of their capability of supplying loads in absence of a connection to the main grid, ImGs provide a flexible solution for bringing power to remote areas or islands [1, 2, 3, 4, 5]. Furthermore, they can be used for improving the robustness of the main grid, e.g. by guaranteeing power supply after the occurrence of an islanding event. Self-sufficient and flexible generation islands also promote the deregulation of the energy market and they have been advocated as a key component of future smart power systems [6]. One of the key issues of ImGs is scalability, i.e. how to add and remove DGUs without compromising the safe operation of the whole system. This problem is not trivial, as voltage stability must be guaranteed by regulating the Voltage-Source Converter (VSC) of individual DGUs. Furthermore, in order to make online computations grow nicely with the ImG size, decentralized control architectures (where each DGU is equipped with a local regulator) must be used [7, 8, 9]. As each local controller measures variables of the corresponding DGU only, the plugging-in or -out of a DGU can easily destabilize the whole ImG if the control layer is not properly updated [10]. In order to overcome this problem, in [1, 10] the authors present a methodology for designing local primary regulators in order to allow Plug-and-Play (PnP) operations [11, 12] while preserving voltage and frequency stability of the overall ImG. More precisely, when a DGU issues a plug-in or -out request, the safety of the operation is first checked by solving optimization problems that involve only the corresponding DGU and parameters of power lines connecting it to the neighboring units. If the test is passed, stability-preserving regulators are synthesized for the DGU and its neighbors. Compared to other decentralized primary control architectures for ImGs, such as the combination of inner loops and droop controllers [3, 13, 14], PnP controllers are simpler and they are not based on the idea of mimicking regulators for inertial generators. Moreover, differently from decentralized regulators based on robust control [7, 8], the knowledge of the whole ImG model is not required for local control design. Rather, just the parameters of power lines are used in the synthesis algorithm.

In this paper, we adapt PnP controllers proposed in [1, 10] for achieving several goals and we validate the control architecture through experiments performed on an AC ImG facility. First, since the method in [1] allows to compute local stabilizing controllers for ImGs arranged in *load-connected* topologies only (i.e. where local loads appear at the output terminals of each DGU), we propose a simple procedure for mapping *bus-connected* ImGs (i.e. networks with a common load, supplied by all the DGUs - which are frequently found in several applications) into their equivalent load-connected models. Secondly, we enhance basic PnP controllers with virtual impedance loops, which are needed for setting the output impedance of bus-connected VSCs. Thirdly, we equip the PnP-controlled ImG with a secondary coordinated control layer for voltage tracking at the load bus and sharing of reactive power among parallel VSCs. Notably, since secondary controllers are commonly used in ImGs [7], we aim to show how they can be easily coupled with low-level PnP controllers for improving performance without compromising the collective ImG stability.

We conduct several experiments on a bus-connected ImG and assess performance of PnP controllers in tracking set-point voltages. Besides showing the negligible impact of transients when the addition/removal of a DGU is performed, we also demonstrate the good behavior of the closed-loop ImG in presence of both linear and nonlinear loads.

The paper is organized as follows. In Section 2, we recall the electrical model of a load-connected ImG and derive the formulae for computing the equivalent load-connected network of a bus-connected one. In Section 3, we briefly describe the PnP control approach in [1] and show how to extend the design of PnP voltage and frequency regulators to the case of bus-connected ImGs. In Section 4, the secondary coordinated control layer is presented. Section 5 is devoted to the assessment, through experiments, of PnP control alone and in combination with the secondary coordinated control layer. Some conclusions are presented in Section 6.

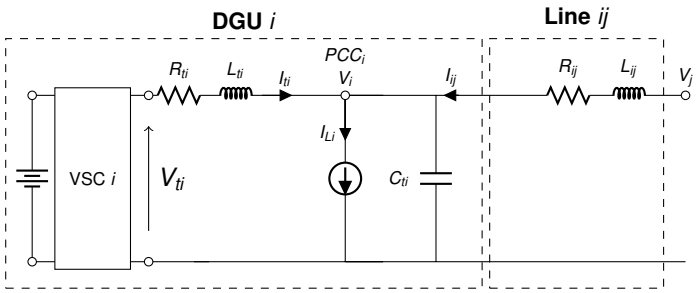

Figure 1: Equivalent single-phase electrical scheme of DGU i and power line ij in a load-connected ImG.

2 Microgrid models

2.1 Load-connected DGU model

In this Section, we present the electrical ImG model considered in [1] for designing decentralized voltage and frequency PnP regulators. We assume three-phase electrical signals without zero-sequence components and balanced network parameters. The single-phase equivalent scheme of DGU i is shown in Figure 1. As in [1], we have a DC voltage source for modeling a generic renewable resource, and a VSC is controlled in order to supply a *local load* (hence the name load-connected topology) connected to the Point of Common Coupling (PCC) through an RLC filter. Moreover, we assume that loads I_{Li} are unknown and we treat them as exogenous disturbances [8].

Assume now that our ImG is composed of N DGUs. We can define the set $\mathcal{V}_{DGU} = \{1, \dots, N\}$, and call two DGUs *neighbors* if there is a power line connecting their PCCs. In particular, we denote the subset of neighbors of DGU i with $\mathcal{N}_i \subset \mathcal{V}_{DGU}$. We further observe that the neighboring relation is symmetric (i.e. $j \in \mathcal{N}_i$ implies $i \in \mathcal{N}_j$).

Let ω_0 be the reference network frequency. By exploiting Quasi Stationary Line (QSL) approximation of power lines [1, 15], we get the following DGU model in dq reference frame (rotating with speed ω_0) [1, 16]

$$\text{DGU } i\text{:} \quad \begin{cases} \dfrac{\mathrm{d}}{\mathrm{d}t} V_i^{dq} = -\mathrm{i}\omega_0 V_i^{dq} + \dfrac{I_{ti}^{dq}}{C_{ti}} - \dfrac{I_{Li}^{dq}}{C_{ti}} + \displaystyle\sum_{j \in \mathcal{N}_i} \frac{1}{C_{ti}} \left(\frac{V_j^{dq} - V_i^{dq}}{Z_{ij}} \right) & \text{(1a)} \\ \dfrac{\mathrm{d}}{\mathrm{d}t} I_{ti}^{dq} = -\left(\dfrac{R_{ti}}{L_{ti}} + \mathrm{i}\omega_0 \right) I_{ti}^{dq} - \dfrac{V_i^{dq}}{L_{ti}} + \dfrac{V_{ti}^{dq}}{L_{ti}} & \text{(1b)} \end{cases}$$

where quantities V_i, V_j, I_{ti}, I_{Li}, V_{ti}, R_{ti}, C_{ti} and L_{ti} are shown in Figure 1. Notably, (i) V_i and I_{ti} represent the i-th PCC voltage and filter current, respectively, (ii) V_{ti} is the command input to the corresponding VSC, (iii) R_{ti}, L_{ti} and C_{ti} are the converter parameters, and (iv) V_j indicates the voltage at the PCC of each neighboring DGU $j \in \mathcal{N}_i$. Moreover, $Z_{ij} = R_{ij} + \mathrm{i}\omega_0 L_{ij}$, where R_{ij} and L_{ij} are, respectively, the resistance and impedance of the three-phase power line connecting DGUs i and j. Finally, we indicate with $\mathcal{G}_{lc} = (\mathcal{V}_{DGU}, \mathcal{E}_{lc}, W_{lc})$ the directed electric graph associated to the load-connected ImG (see, e.g., Figure 2-b), where weights W_{ij} of edges $e_{ij} \in \mathcal{E}_{lc}$ coincide with the admittances $\frac{1}{Z_{ij}}$ in (1a).

2.2 From bus-connected to load-connected topology

The fact that the method in [1] allows to design stabilizing PnP controllers for load-connected ImGs only, does not represent a limitation. In fact, as shown in [17, 16], arbitrary interconnections of loads and DGUs can always be mapped into their equivalent load-connected topologies by means of Kron reduction [18]. Kron reduction is a well-known method for simplifying linear

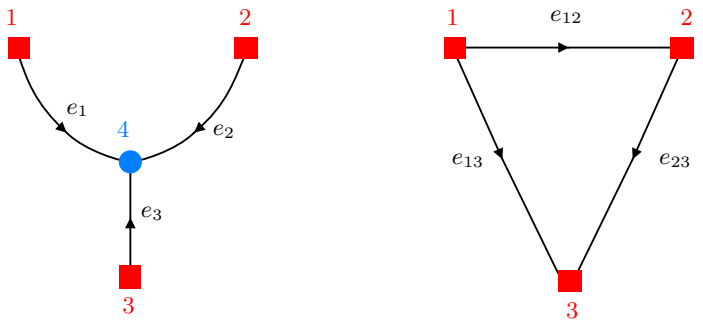

Figure 2: Graphs of a bus-connected ImG with 3 DGUs (on the left) and its equivalent load-connected network (on the right). Red squares indicate DGUs with corresponding local loads I_{Li} (boundary nodes), while the blue circle denotes the unique load at the common bus (internal node).

electrical networks while preserving the behavior of electrical variables at target nodes (also called *boundary nodes*). In particular, Kron reduction provides an algebraic procedure for computing (i) the corresponding load-connected topology (where only boundary nodes are connected) of the original, arbitrarily connected network, (ii) the admittances of the new edges and (iii) the equivalent currents injected at boundary nodes accounting for the effect of the currents of the eliminated nodes (also called *internal nodes*) in the original network. An example of the transformation is provided in Figure 2.

Since several works from the literature consider ImGs arranged in bus-connected topology [19, 20, 21], we are interested in mapping these topologies into the corresponding load-connected ones. While it goes without saying that Kron reduction can also be applied to this aim (by eliminating the node representing the load bus[1]), it requires the inversion of an admittance matrix. In the following, instead, we provide an equivalent procedure, leading to explicit formulae, for computing the admittances of the power lines of the corresponding load-connected network (e.g. the weights of edges e_{12}, e_{13} and e_{23} in Figure 2). This method relies on Kirchhoff's Current Law (KCL), Kirchhoff's Voltage Law (KVL) and QSL approximation.

As a starting point, let us consider a bus-connected ImG with N DGUs feeding a common load (I_L) connected to the Point of Load (PoL). Figure 3 provides an example with $N = 3$ and shows parameters R_i, L_i and currents I_i characterizing each DGU. As usual, we assume balanced lines. By applying KCL and KVL in the *abc*-frame and performing the Park's transformation [22], we have that the dynamics of DGU i in dq-coordinates, with $\omega = \omega_0$, are described by

$$\frac{\mathrm{d}}{\mathrm{d}t} V_i^{dq} = \frac{I_{ti}^{dq}}{C_{ti}} - \frac{I_i^{dq}}{C_{ti}} - \mathrm{i}\omega_0 V_i^{dq} \tag{2}$$

and (1b). For $1 \leq j \leq N$, $j \neq i$, it holds

$$V_i^{dq} - V_j^{dq} = R_i I_i^{dq} + L_i \frac{\mathrm{d}}{\mathrm{d}t} I_i^{dq} + \mathrm{i}\omega_0 L_i I_i^{dq} - R_j I_j^{dq} - L_j \frac{\mathrm{d}}{\mathrm{d}t} I_j^{dq} - \mathrm{i}\omega_0 L_j I_j^{dq}. \tag{3}$$

By virtue of QSL approximations (see [1, 15]), in (3), we set $\frac{\mathrm{d}}{\mathrm{d}t} I_i^{dq} = 0$, $\forall i \in \mathcal{V}_{DGU}$. Hence, equation (3) becomes

$$V_i^{dq} - V_j^{dq} = R_i I_i^{dq} + \mathrm{i}\omega_0 L_i I_i^{dq} - R_j I_j^{dq} - \mathrm{i}\omega_0 L_j I_j^{dq}\,, \qquad 1 \leq j \leq N,\ j \neq i.$$

[1]Node 4 in the example in Figure 2.

Next, defining $Z_i = R_i + \mathrm{i}\,\omega_0 L_i$, one gets

$$I_j^{dq} = \frac{V_j^{dq} - V_i^{dq}}{Z_j} + \frac{Z_i}{Z_j} I_i^{dq}\,, \qquad 1 \le j \le N,\ j \neq i. \tag{4}$$

Applying KCL at the PoL, we have

$$I_i^{dq} + \sum_{j \neq i} I_j^{dq} = I_L^{dq} \tag{5}$$

and, inserting (4) in (5), we obtain

$$I_i^{dq} = \frac{I_L^{dq}}{\left(1 + \sum_{j\neq i} \frac{Z_i}{Z_j}\right)} + \left(\sum_{j\neq i} \frac{1}{Z_j}\right) \frac{V_i^{dq}}{\left(1 + \sum_{j\neq i} \frac{Z_i}{Z_j}\right)} - \sum_{j\neq i} \frac{V_j^{dq}}{Z_j} \frac{1}{\left(1 + \sum_{j\neq i} \frac{Z_i}{Z_j}\right)}. \tag{6}$$

Observing that, in the formula above

$$\frac{1}{\left(1 + \sum_{j\neq i} \frac{Z_i}{Z_j}\right)} = \frac{1}{\left(Z_i \sum_{k=1}^{N} \frac{1}{Z_k}\right)},$$

we can introduce the following notation

$$\frac{1}{Z_{ij}} = \frac{1}{Z_j Z_i \sum_{k=1}^{N} \frac{1}{Z_k}}\,, \forall j \neq i,$$

which implies

$$\left(\sum_{j\neq i} \frac{1}{Z_j}\right) \frac{1}{\left(Z_i \sum_{k=1}^{N} \frac{1}{Z_k}\right)} = \sum_{j\neq i} \frac{1}{Z_{ij}}. \tag{7}$$

At this point, by replacing (7) in (6), and then substituting the resulting expression into (2), one gets that the dynamics of V_i^{dq} have the form (1a). In other words, we have derived the equivalent load-connected model of a bus-connected ImG with complex power lines admittances $1/Z_i$, $i = 1, ..., N$. Notably, the weights of the equivalent load-connected network (indicated with $1/Z_{ij}$ $i, j = 1, ..., N,\ i \neq j$, as in (1a)) are given by (7), while the effect of the eliminated node (i.e. the PoL) at the i-th PCC is accounted by the following injected current

$$I_{Li}^{dq} = \frac{I_L^{dq}}{\left(Z_i \sum_{k=1}^{N} \frac{1}{Z_k}\right)}. \tag{8}$$

Finally, we highlight that, since admittances $1/Z_{ij}$ $i, j = 1, ..., N,\ i \neq j$ are all nonzero, the described transformation always returns a fully connected reduced network (see the example in Figure 2-b, where each pair of distinct nodes is connected by a unique edge).

3 Plug-and-play primary control layer

3.1 Control architecture

Figure 4 shows a bus-connected DGU, equipped with a decentralized PnP controller. Each local regulator exploits measurements of the voltage V_i^{dq} at the PCC and the current I_{ti}^{dq}, in order to control the voltage V_{ti}^{dq} at the VSC i and make V_i^{dq} track a reference signal. We notice that the proposed controller is multivariable, where the only tunable parameter is the matrix gain K_i in Figure 4. Compared to common solutions found in the literature [3, 21], the proposed scheme breaks the hierarchical structure composed of inner current and voltage loops and droop control.

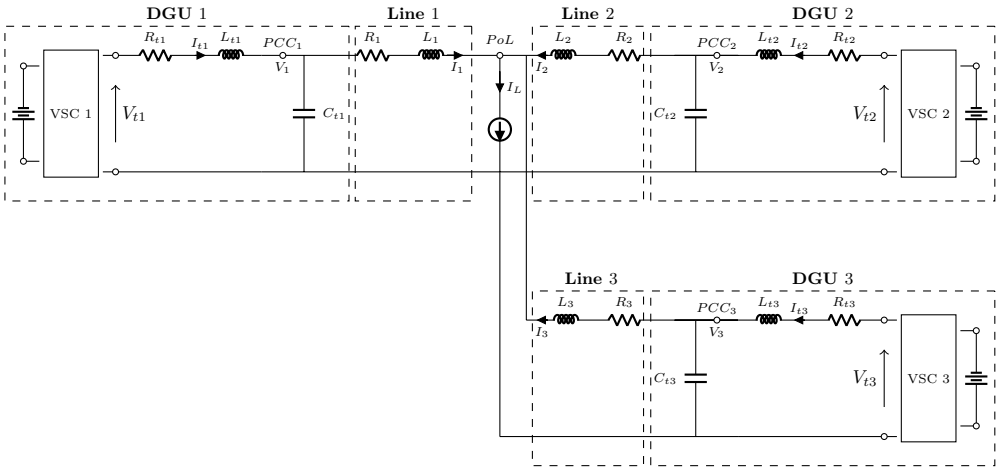

Figure 3: Electrical scheme of a bus-connected ImG composed of three DGUs and a common unmodeled load.

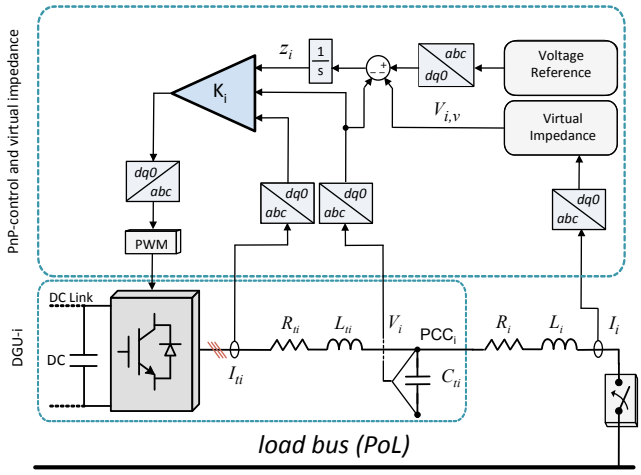

Figure 4: Bus-connected DGU equipped with local PnP regulator and virtual impedance loop.

However, as in single-input single-output current and voltage loops, feedback information consists of the current provided by the VSC and the voltage at the PCC. Most importantly, the presence of the integrators guarantees tracking of constant set-point references in the dq-frame, and hence of three-phase sinusoidal quantities in the abc-frame.

Figure 4 also reveals the presence of a virtual impedance loop. Virtual impedance is a widely used tool in control of parallel interconnected VSCs [23, 21]. Its employment is instrumental for lowering the circulating currents between DGUs generated by line-impedance unbalance and mismatch in inverter parameters. In practice, as shown in Figure 4, the virtual impedance reduces the voltage reference by a term proportional to the line current, thus mimicking an RL impedance connected in series to the output filter of the inverter. We also highlight that virtual resistances and inductances should be chosen sufficiently large so as to outnumber such uncertainties in the electrical parameters. In contrast with a physical device, a virtual impedance has no power losses. In [23, 21], the virtual impedance is expressed in $\alpha\beta$-coordinates. Similarly, we can model it in

dq-coordinates as follows:

$$\begin{aligned} V_{i,v}^d &= R_{i,v} I_i^d + L_{i,v} \frac{\mathrm{d}I_i^d}{\mathrm{d}t} - \omega_0 L_{i,v} I_i^q \\ V_{i,v}^q &= R_{i,v} I_i^q + L_{i,v} \frac{\mathrm{d}I_i^q}{\mathrm{d}t} + \omega_0 L_{i,v} I_i^d \end{aligned} \tag{9}$$

where $R_{i,v}$ and $L_{i,v}$ are the virtual resistance and inductance parameters and $V_{i,v}$ and I_i are the voltage and current in the dq-frame shown in Figure 4.

3.2 Plug-and-play design of local controllers

In the following, we first summarize the PnP algorithm in [1] for designing the matrix gain K_i in Figure 4. Then, since the algorithm in [1] assumes load-connected ImGs only, we exploit the result derived in Section 2.2 to apply the above methodology to bus-connected networks.
PnP design of local controllers proposed in [1] guarantees overall voltage and frequency stability, with the main advantage that a global ImG model is not required in any design step. Moreover, individual DGUs can test if the addition/removal of a subsystem is dangerous for the ImG stability by following the procedure below.

Assume that the plug-in of a DGU (say DGU i) is required. This new unit issues a plug-in request to its future neighboring DGUs j, $j \in \mathcal{N}_i$, and then solves the Linear Matrix Inequality (LMI) test (19) in [1], which is a convex optimization problem depending only upon the parameters of power lines ij, $j \in \mathcal{N}_i$ (e.g., R_{ij} and L_{ij} in Figure 1). If the optimization is feasible, the above test returns the matrix gain K_i. Moreover, since also DGUs $j \in \mathcal{N}_i$ will have a new neighbor, they must retune their controller, so as to account for the presence of new coupling terms. The update of the j-th controller is done by solving an LMI problem analogous to the one solved for DGU i. If one of the above LMI tests is unfeasible, the plug-in of DGU i is denied. Otherwise, DGU i (equipped with controller K_i) can be connected to the network without compromising the collective voltage and frequency stability of the ImG.

Unplugging of a DGU (say DGU m) follows a similar procedure. As line mk is disconnected, only DGUs k, $k \in \mathcal{N}_m$ must successfully recompute their local controllers before allowing the disconnection of DGU k (see [1] for details).

Let us consider now the case in which we have a bus-connected ImG. Whenever we want to plug-in a new DGU (say DGU i), the first step is to compute the line impedances between DGU i and each DGU j, $j \in \mathcal{V}_{DGU} \setminus \{i\}$, using (7). Subsequently, the LMI test (19) in [1] must be successfully solved for all the DGUs, in order to allow the safe connection of DGU i. On the other hand, if only one of these tests LMI is infeasible, the plug-in of DGU i is denied. Unplugging of a DGU can be performed in a similar way.

Remark 1. *The procedure for handling plug-in/-out operations when the original network is arranged either in a load- or bus-connected topology can be simplified as follows. Let us assume that the hot plug-in (i.e. the plug-in in real-time) of DGU i has been allowed and scheduled at a future time $\bar{t}$. At the same time instant, DGUs j (with $j \in \mathcal{N}_i$ if the ImG is load-connected, or $j \in \mathcal{V}_{DGU} \setminus \{i\}$ if the ImG is bus-connected) will start using the new gains. Retuning of gains K_j, however, could be avoided if previous gains are still feasible for the corresponding LMI test. In other words, for such DGUs j, one can check if matrix gains K_j working for $t < \bar{t}$ still fulfill the constraints of their corresponding optimization problem (19) in [1]. Preserving previously designed controllers, in fact, has the advantage of reducing perturbations on electrical signals right after $\bar{t}$, which might be caused by controller switching.*

In a similar way, if DGU m is disconnected, the retuning of controllers of DGUs k (with $k \in \mathcal{N}_m$ or $k \in \mathcal{V}_{DGU} \setminus \{m\}$ if the ImG is load- or bus- connected, respectively) can be avoided if the LMI test (19) in [1] is feasible for previously designed matrix gains K_k.

3.3 Clock synchronization for primary control

The computation of VSC commands assumes that all clocks of local controllers, used for performing *abc* to *dq* transformations, are synchronized. As also highlighted in [7], each DGU can include a crystal oscillator that generates the angular phase $\theta(t) = \int_0^t \omega_0 \, d\tau$. However, if the local oscillators are not synchronized, the local angular phase is given by $\theta_i(t) = \theta(t) + \theta_{i,0}$, where $\theta_{i,0}$ is the initial offset. In [7], the authors propose a synchronization using GPS radio clock, which could achieve an accuracy higher than 1μs [24].

An alternative solution is to synchronize clocks using communication between controllers. This operation can be performed quite rarely because, as noted in [7], currently available crystal oscillators are characterized by high accuracy (from 2 μs to 20 ps in a year [25]). Moreover, synchronization can be done through packet networks, using either a distributed protocol (e.g. Berkeley algorithm [26]) or approaches based on all-to-all communication, such as instantaneous averaging [27].

If an ImG is equipped with primary PnP regulators, prior to allowing the plug-in of a new DGU, it is mandatory to synchronize it with all the ones already connected to the PoL. Therefore, in the experiments described in Section 5, we let each new DGU estimate $\theta_{i,0}$ by computing the average angular phases of all the other DGUs.

3.4 Harmonic compensation by tuning the PnP control bandwidth

Besides collective voltage and frequency stability, PnP design can guarantee good harmonic compensation, even in absence of low-level resonant controllers (described, e.g., in [21]). In fact, as explained in [1], one can also shape, in a desired fashion, the singular values of the overall closed-loop ImG. More specifically, in order to provide suitable attenuation of the 5-th, 7-th and 11-th harmonics in *abc*-frame, we design primary PnP controllers that attenuate the 4-th, 6-th and 10-th harmonics in the rotating *dq*-frame. An example is provided in Figure 5 for an ImG with two DGUs. The singular values of closed-loop ImG transfer function from voltage references to the voltages at the PCCs are represented in Figure 5a. Similarly, the singular values of the transfer function from voltage references to the currents in the filters are given in Figure 5b. Notice that good attenuation can be obtained also when couplings between DGUs are accounted for. In fact, assuming $f_0 = 50$ Hz, from Figure 5a, the attenuation of the 5-th, 7-th and 11-th voltage harmonics is 50 dB, 60 dB and 70 dB, respectively.

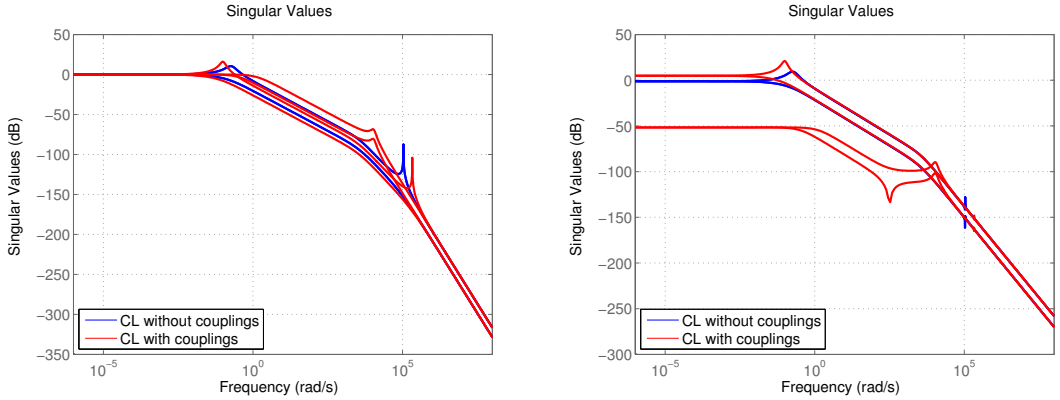

(a) Singular values of the transfer function matrix from *dq* voltage references to *dq* voltages at the PCCs.

(b) Singular values of the transfer function matrix from *dq* voltage references to *dq* currents in the filters.

Figure 5: Singular values for the closed-loop ImG with two DGUs.

4 Coordinated control

Using PnP controllers described in Section 3.2, we are able to guarantee voltage and frequency stability for the overall ImG. Notably, each local controller regulates the voltage at the corresponding PCC, according to the following reference in the *abc*-frame

$$\begin{aligned} V^*_{i_a}(t) &= V^*_i \sin\left(\omega_0 t + \phi^*_i\right) \\ V^*_{i_b}(t) &= V^*_i \sin\left(\omega_0 t + \phi^*_i - \frac{2\pi}{3}\right) \\ V^*_{i_c}(t) &= V^*_i \sin\left(\omega_0 t + \phi^*_i + \frac{2\pi}{3}\right). \end{aligned} \tag{10}$$

In bus-connected ImGs, one can indirectly control voltage and frequency at the PoL by choosing voltages V^*_i, $i = 1, \ldots, N$ in (10). In several control architectures, the use of a Power-Management System (PMS) has been proposed for this purpose (see for example [7]). The basic idea is to compute voltage references such that each DGU injects prescribed active and reactive power. The PMS must be run in real-time in order to maintain a prescribed power flow, even if loads change. In the following, we propose a distributed secondary control layer capable to guarantee (i) a desired voltage at the PoL, and (ii) sharing of reactive power injections among DGUs.

4.1 Voltage tracking at the PoL

Let us indicate the desired PoL voltage with $V^*_{PoL}\angle 0$[2]. In absence of loads, in order to guarantee the reference at the PoL, we could set, in (10), $V^*_i = V^*_{PoL}$ and $\phi^*_i = 0$. However, due to the presence of time-varying loads, V^*_i and ϕ^*_i must be adapted over time. We propose that each DGU changes its set-point according to

$$\begin{aligned} V^*_{i_a}(t) &= (V^*_{PoL} + \Delta V_{PoL}) \sin\left(\omega_0 t + \Delta\phi_{PoL}\right) \\ V^*_{i_b}(t) &= (V^*_{PoL} + \Delta V_{PoL}) \sin\left(\omega_0 t + \Delta\phi_{PoL} - \frac{2\pi}{3}\right) \\ V^*_{i_c}(t) &= (V^*_{PoL} + \Delta V_{PoL}) \sin\left(\omega_0 t + \Delta\phi_{PoL} + \frac{2\pi}{3}\right), \end{aligned} \tag{11}$$

instead of using (10). The next aim is to compute ΔV_{PoL} and $\Delta\phi_{PoL}$ in order to keep PoL voltage close to its reference. Since we can not measure the voltage at the PoL, we estimate its amplitude and phase averaging local measurements

$$V_{PoL} = \sum_{i=1}^{N} \frac{V_{PoL,i}}{N} \qquad \phi_{PoL} = \sum_{i=1}^{N} \frac{\phi_{PoL,i}}{N} \tag{12}$$

where $V_{PoL,i}$ and $\phi_{PoL,i}$ are computed by each DGU from V_i and I_i (shown in Figure 4) as follows

$$V_{PoL,i} = \sqrt{(V^d_{PoL,i})^2 + (V^q_{PoL,i})^2} \qquad \phi_{PoL,i} = \frac{V^q_{PoL,i}}{V^d_{PoL,i}}, \tag{13}$$

where

$$\begin{aligned} V^d_{PoL,i} &= V^d_i + \omega_0 L_i I^q_i \\ V^q_{PoL,i} &= V^q_i - \omega_0 L_i I^d_i. \end{aligned}$$

We equip each DGU with the local controller in Figure 6 for computing ΔV_{PoL} and $\Delta\phi_{PoL}$ in (11). We note that the controller in Figure 6 is replicated in each DGU instead of being unique for the whole ImG. As shown in [28], replicating the controller has several advantages when the communication latency increases. Differently from the PnP control architecture that is completely

[2]Without loss of generality, the phase has been assumed equal to zero.

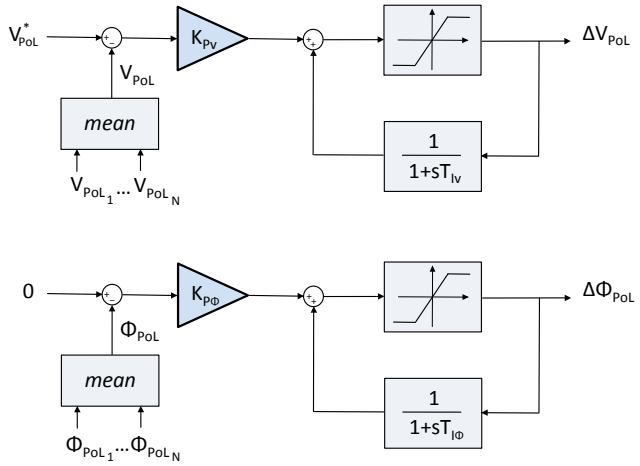

Figure 6: Coordinated control layer: computation of correction terms ΔV_{PoL} and $\Delta\phi_{PoL}$. Parameters K_{PV} and $K_{P\phi}$ are the voltage and phase proportional coefficients, while T_{IV} and $T_{I\phi}$ are the voltage and phase integral time constants.

decentralized, the secondary layer of controllers is distributed as it needs a communication network in order to exchange values $V_{PoL,i}$ and $\phi_{PoL,i}$, and then to compute locally the averages (12). Formula (12) requires a fully connected communication network, as all measurements $V_{PoL,i}$ and $\phi_{PoL,i}$ have to be broadcasted to all DGUs. However, this limitation could be avoided by resorting to distributed algorithms, based on consensus strategies, for tracking the average of time-varying signals [29]. Indeed, these methods only require sparse, yet connected, networks. In Figure 7 we show the flow of information for the proposed coordinated controller. Each controller in Figure 6

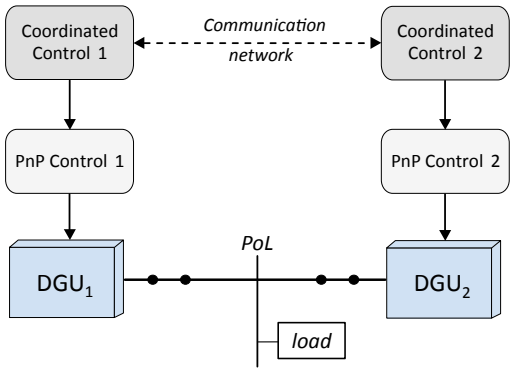

Figure 7: Scheme of the coordinated control.

is a PI regulator with an anti-windup scheme accounting for saturations on ΔV_{PoL} and $\Delta\phi_{PoL}$. These saturations are needed to limit the amplitude and phase deviations, thus preventing the opening of breakers connecting inverters to the PoL. When saturations are not active, ΔV_{PoL} and $\Delta\phi_{PoL}$ are computed through the standard PI formulae

$$\Delta V_{PoL}(t) = K_{PV}(V^*_{PoL} - V_{PoL}(t)) + K_{IV}\int_0^t (V^*_{PoL} - V_{PoL}(\tau))\, d\tau \tag{14}$$

$$\Delta\phi_{PoL}(t) = K_{P\phi}(0 - \phi_{PoL}(t)) + K_{I\phi}\int_0^t (0 - \phi_{PoL}(\tau))\, d\tau. \tag{15}$$

Next, we discuss the tuning of PI parameters. The integral time constants $T_{IV} = K_{PV}/K_{IV}$ and $T_{I\phi} = K_{P\phi}/K_{I\phi}$ in Figure 6 are chosen to make the corresponding PI control loop sufficiently slower than the inner PnP control loop. To this aim, we use the following first-order approximation

of each DGU equipped with the corresponding stabilizing PnP controller

$$V_i^d = \frac{1}{1+sT_i^d}V_i^{*d} \qquad V_i^q = \frac{1}{1+sT_i^q}V_i^{*q}.$$

Furthermore, since the overall PnP architecture is stable and due to the presence of output impedance for each DGU, we can also state that

$$V_{PoL,i}^d = \frac{\mu_i^d e^{-s\tau_i^d}}{1+sT_i^d}V_i^{*d} \qquad V_{PoL,i}^q = \frac{\mu_i^q e^{-s\tau_i^q}}{1+sT_i^q}V_i^{*q}$$

where μ_i^d, μ_i^q, τ_i^d and τ_i^q depend on the output impedance. Using (13), assuming $\tau_i = \tau_i^d \approx \tau_i^q$, $T_i = T_i^d \approx T_i^q$ and setting $\mu_i = \sqrt{(\mu_i^d)^2 + (\mu_i^q)^2}$, we obtain

$$V_{PoL,i} = \frac{\mu_i e^{-s\tau_i}}{1+sT_i}V_i^* \qquad \phi_{PoL,i} = \phi_i^*. \tag{16}$$

Therefore, using (16) and (12), we can provide a linear model of the effect of V_i^* and ϕ_i^* on V_{PoL} and ϕ_{PoL}, respectively. Furthermore, since $V_i^* = V_{PoL}^* + \Delta V_{PoL}$ and $\phi_i^* = 0 + \Delta\phi_{PoL}$, we also obtain a small-signal model of the effect of ΔV_{PoL} and $\Delta\phi_{PoL}$ on V_{PoL} and ϕ_{PoL}, respectively.
As regards the phase deviation, since $\phi_{PoL,i} = \phi_i^* = \Delta\phi_{PoL}$, we can easily derive a simplified model as

$$\phi_{PoL} = \frac{\Delta\phi_{PoL}}{N}$$

which can be used for computing the PI control action in (15).
For deriving a simplified model of the amplitude deviation, the closed-loop DGU dynamics in the first control layer must be considered. The second control layer should act mostly when the first control layer is at steady-state. Hence, using (16), we can write a local approximate dynamics as

$$V_{PCC,i} = \frac{\mu_i e^{-s\tau_{PCC}}}{1+sT_{PCC}}V_i^* = \frac{\mu_i e^{-s\tau_{PCC}}}{1+sT_{PCC}}(V_{PCC}^* + \Delta V_{PCC})$$

where $\tau_{PoL} = \max(\tau_1, \ldots, \tau_N)$ and $T_{PoL} = \max(T_1, \ldots, T_N)$. Next, using (12), we can derive

$$V_{PoL} = \frac{\mu e^{-s\tau_{PoL}}}{1+sT_{PoL}}V_{PoL}^* + \frac{\mu e^{-s\tau_{PoL}}}{1+sT_{PoL}}\Delta V_{PoL}$$

where $\mu = \sum_{i=1}^N \frac{\mu_i}{N}$. In conclusion, we tune the gains of the PI controller assuming the system under control has the transfer function

$$\frac{V_{PoL}}{\Delta V_{PoL}} = \frac{\mu e^{-s\tau_{PoL}}}{1+sT_{PoL}}.$$

4.2 Sharing of reactive power

Inner PnP regulators complemented with coordinated controllers for voltage tracking at the PoL cannot alone guarantee accurate reactive power sharing among DGUs. For this reason, we propose an additional coordinated controller dedicated to this aim. We assume that DGUs are connected to the PoL through mostly inductive lines[3]. In this case, the sharing of the reactive power is due to the amplitude of the voltages [30, 31]. Therefore, we propose to change the amplitude of the set-point for each DGU as

$$V_i^* = V_{PoL}^* + \Delta V_{PoL} + \Delta V_i^Q, \tag{17}$$

where V_{PoL}^* is the reference for voltage at PoL, ΔV_{PoL} is computed as in (14) and ΔV_i^Q is a voltage correction to guarantee reactive power sharing. Voltage ΔV_i^Q is computed by the PI controller

[3]Results can be easily adapted to the case of lines that are mostly resistive.

equipped with anti-windup shown in Figure 8. In particular, when the saturation on ΔV_i^Q is not active, one has

$$\Delta V_i^Q(t) = K_{PQ}(Q(t) - Q_i(t)) + K_{IQ} \int_0^t (Q(\tau) - Q_i(\tau))\, d\tau$$

where Q_i is the reactive power injected by the local DGU and $Q(t)$ is the average of the injected reactive powers. The PI regulator in Figure 8 is replicated in each DGU. Moreover, the whole control layer requires the communication network displayed in Figure 7 since all units must exchange the values of reactive power $Q_i(t)$ for computing locally average $Q(t)$.

Similarly to what we have done for the PI regulators in Figure 6, each integral time constant T_{IQ}

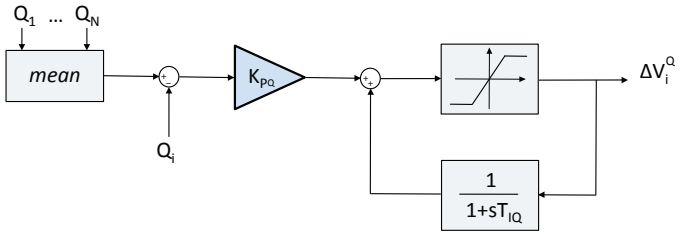

Figure 8: Control scheme for the computation of ΔV_i^Q. Parameters K_{PQ} and T_{IQ} are the reactive power proportional term and the reactive power time constant, respectively.

is designed to make the corresponding PI controller slower than the inner PnP ones.

5 Experimental results

5.1 Microgrid setup

We tested the performance of the proposed approach using the ImG platform in Figure 9a; it consists of three *Danfoss* inverters (2.2kVA with *RLC* filters), a dSPACE1103 control board and LEM sensors. Inverters operate in parallel to emulate DGUs while different load conditions are obtained by connecting to the bus resistive loads and/or a diode rectifier. All the inverters are supplied by a DC source generator, therefore neither renewable sources nor energy storage devices are present in the experimental setup. Although this does not allow to study the effect of power fluctuations from renewable sources, the reliability of our experimental validation is guaranteed by the fact that, in general, changes in the power supplied by renewables take place at a timescale that is slower than the one we are interested in for stability analysis.

The controllers have been implemented in Simulink and compiled to the dSPACE system in order to command the inverter switches at a frequency of 10 kHz. Although the dSPACE platform is unique (see also Figure 9b), separate local controllers for each inverter were implemented so as to guarantee the control architecture can be implemented in a real distributed inverter system. The scheme of the experimental setup is depicted in Figure 9a.

In the performed experiments, we make sure that, at time $t = 0$ s, all the controllers are already activated so that all the voltages at the PCCs start from their reference value (230 V).

The control and electrical parameters are reported in Table 1. Furthermore, we highlight that the clocks of local controllers have been synchronized using the procedure described in Section 3.3.

In the following sections, we validate primary PnP controllers under linear, unbalanced and nonlinear load conditions, as well as the combination of such primary layer with the proposed secondary coordinated controllers.

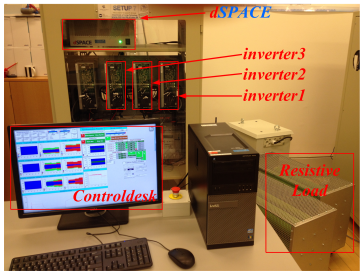

(a) Experimental ImG setup.

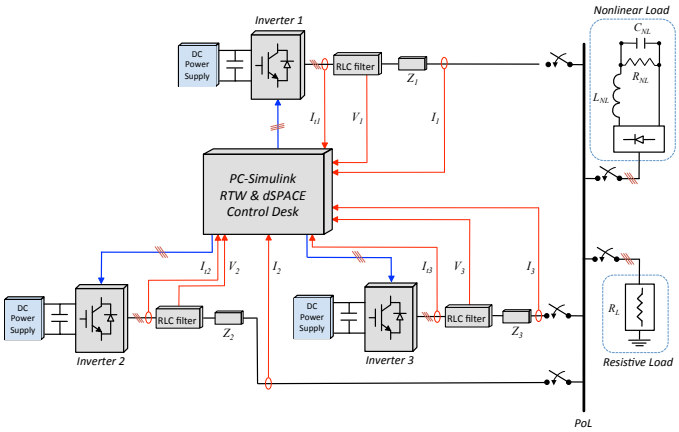

(b) Scheme of the experimental setup. Red lines indicate the electrical variables measured at each DGU level. Blue lines represent the control commands to the inverters.

Figure 9: Experimental validation: ImG setup and implemented control scheme.

5.2 Experimental results: plug-and-play control

5.2.1 Voltage regulation at the PCCs with resistive load

In this first experiment, we test the capability of PnP primary controllers to handle connection and disconnection of inverters in a bus-connected ImG. At this stage, coordinated controllers described in Section 4 are not used.

At time $t = 0$ s, the first and second inverter are connected to the bus; since there is no load at the PoL, the RMS voltages at PCCs 1 and 2 (red and green line, respectively, in Figure 10a) coincide with the reference.

At $t = 5$ s, we connect a resistive load ($R = 92\ \Omega$) at the PoL. Consequently, the active powers provided by inverters 1 and 2 increase in order to compensate the load (see Figure 10c). We also notice that the frequencies are promptly restored after the load connection (as shown in Figure 10b).

Since the voltage references at PCCs are fixed, PnP controllers alone cannot guarantee a good voltage regulation at the PoL. Moreover, as recalled in Section 3.1, the presence of a local virtual impedance induces a drop (proportional to the output current) in the corresponding reference voltage. This behavior is shown, for instance, in Figure 10a, where we notice a decrement in the voltages at PCCs 1 and 2 when the load is connected to the PoL (at $t = 5$ s).

At time $t = 15$ s, we plug-in inverter 3. This event induces spikes in the frequencies (see Figure 10b), whose maximal amplitude, however, is less than 0.2 Hz. Moreover, Figure 10c shows that all the inverters provide the same active power to compensate the load.

At times $t = 25$ s and $t = 35$ s, we change the load to $R = 460\ \Omega$ and $R = 154\ \Omega$, respectively. These events generate drops in the active power of more than 50%. Moreover, voltages and frequencies are instantaneously restored (see Figures 10a and 10b). Differently from droop-controllers, PnP controllers are not inertia-based and hence they are capable to provide faster transients.

Finally, at $t = 40$ s and $t = 45$ s we plug-out inverters 3 and 2, respectively, thus eventually feeding the resistive load with inverter 1 only. Also in this case, the impact of the unplugging events on the frequency profile is minor.

5.2.2 Voltage regulation at the PCCs with unbalanced load

In this experiment, we show performance of PnP controllers under unbalanced load conditions. For the sake of simplicity, in Figures 11b-11e we show the evolution of the main electrical quantities

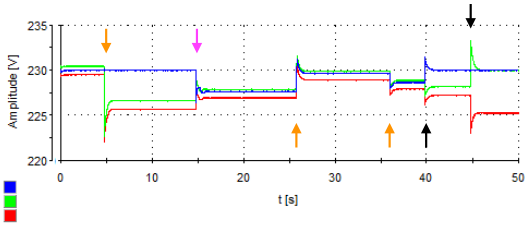

(a) Voltages V_i at the PCCs (phase a).

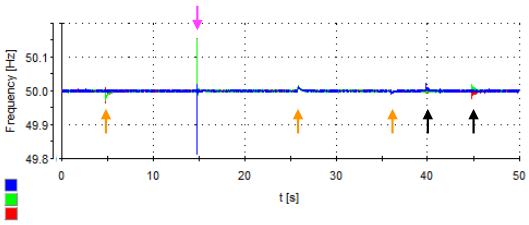

(b) Frequencies (phase a).

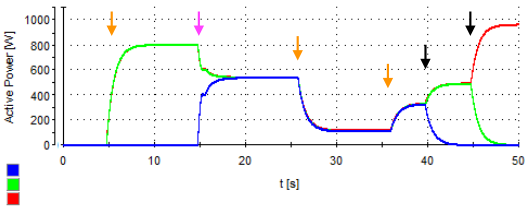

(c) Active power provided by the inverters to the load.

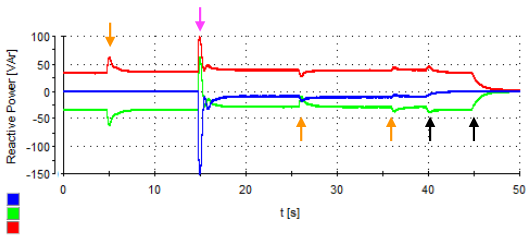

(d) Reactive power provided by the inverters to the load.

Figure 10: Voltage regulation at the PCCs with resistive load (Section 5.2.1). Red, green and blue lines are, respectively, for VSC 1, 2 and 3. Load change, plug-in and unplugging events are indicated with orange, magenta and black arrows, respectively.

of inverter 1 only.

At $t = 0$ s, all the inverters are connected to the PoL and no load is present. Then, at $t = 5$ s we connect a balanced resistive load ($R = 115\ \Omega$) to the common bus. Consequently, inverter 1 provides the output current shown in Figure 11b. At $t = 10$ s, we change phase b of the load to $R = 57\ \Omega$, thus causing the unbalance in the output current 1 shown in Figure 11c. Moreover, the average of the imbalanced ratios [32] for all the inverters is 0.5 % (see Figure 11a). At $t = 15$ s, we change phase c of the load to $R = 230\ \Omega$. As a consequence, in Figure 11d we note an additional unbalance in the output current 1. Moreover, from Figure 11a, we see that the average of the imbalanced ratios increases to 0.75 %. Finally, at $t = 20$ s and $t = 25$ s, we unplug inverters 2 and 3, respectively: since inverter 1 must provide all the power required by the load, the amplitude of its output current increases (Figure 11e). Figure 11a shows that also its imbalance ratio increases to 1 % and then to 1.65 %. However, we notice that, during the whole experiment, the imbalance ratio is quite small and always lower than the maximum value (3 %) recommended by IEEE in [32].

5.2.3 Voltage regulation at the PCCs with nonlinear load

In this scenario, we show features of PnP controllers in presence of nonlinear loads. At time $t = 0$ s, inverters 1 and 2 are connected to the diode rectifier shown in Figure 9b. Hence, the active power provided by inverter 3 is zero (see Figure 12c) and the THD[4] (Total Harmonic Distortion index in [32]) is higher for the voltages at PCCs 1 and 2 (as shown in Figure 12e). At $t = 5$ s, we increase the power required at the PoL by connecting a resistive load ($R = 154\ \Omega$) in parallel with the nonlinear one.

The plugging-in operation of inverter 3 is performed at $t = 15$ s. Notice that the frequencies are promptly restored to the nominal value (variations less than 0.2Hz), total active power is equally shared between all inverters and THDs are reduced for all inverters.

In order to assess the robustness of local PnP regulators to unknown load dynamics, at times

[4]For the sake of simplicity, in Figure 12e we show only the THD indices of phase a of the corresponding PCC voltages.

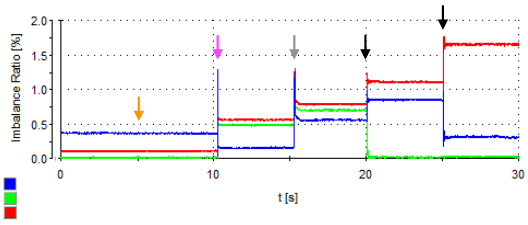

(a) Imbalance ratios. Red, green and blue lines are, respectively, for VSC 1, 2 and 3. Load connection, phase b load unbalancing, phase c load unbalancing and unplugging events are indicated with orange, magenta, grey and black arrows, respectively.

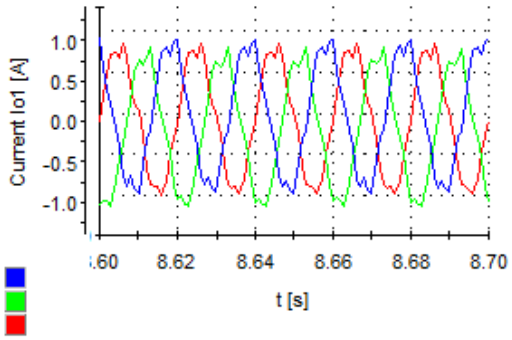

(b) Output current for inverter 1 around time $t = 8.65$ s (effect of balanced load connection at $t = 5$ s).

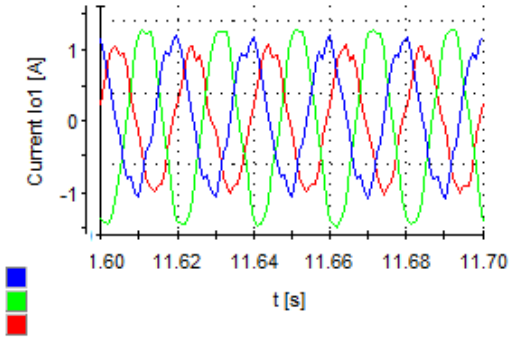

(c) Output current for inverter 1 around time $t = 11.65$ s (effect of load phase b unbalancing at $t = 10$ s).

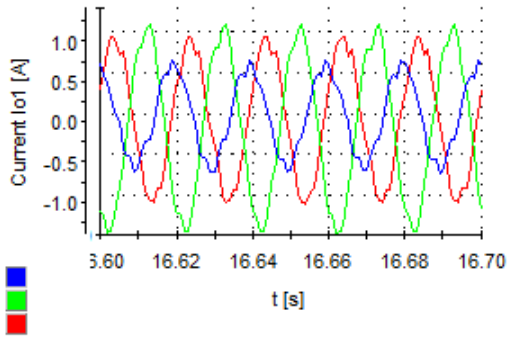

(d) Output current for inverter 1 around time $t = 16.65$ s (effect of load phase c unbalancing at $t = 15$ s).

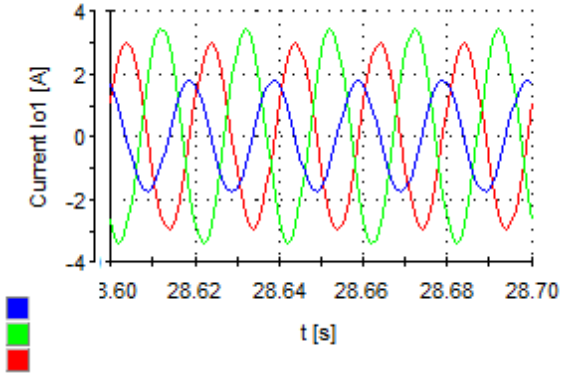

(e) Output current for inverter 1 around time $t = 28.65$ s (after the unplugging of VSCs 2 and 3).

Figure 11: Voltage regulation at the PCCs with unbalanced load (Section 5.2.2).

$t = 25$ s and $t = 35$ s, we switch the resistive load to $R = 460\ \Omega$ and $R = 154\ \Omega$, respectively. Figures 12a and 12b show fast transients of voltages and frequencies at the PCCs.

Finally, at $t = 40$ s and $t = 45$ s, we unplug inverter 3 and 2, respectively. Consequently, the THD of the voltage at PCC 1 increases. However, as shown in Figure 12e, the THD values are

always below the maximum limit (5%) recommended in [32]. Concluding, this experiment reveals that, even in absence of inner resonant controllers, PnP regulators are capable to guarantee high levels of robustness to load variations and harmonic attenuation.

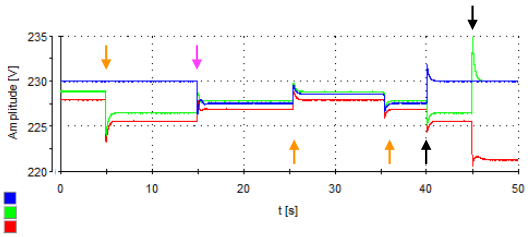

(a) Voltages V_i at the PCCs (phase a).

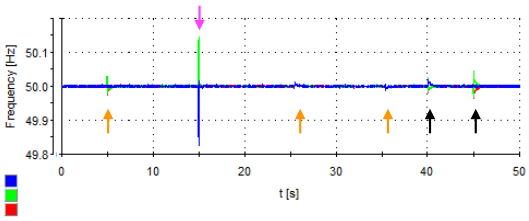

(b) Frequencies (phase a).

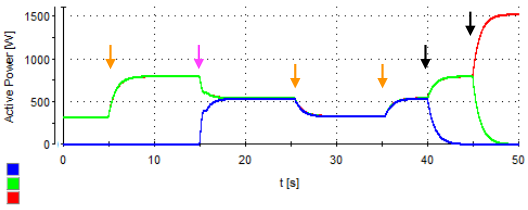

(c) Active power provided by the inverters to the load.

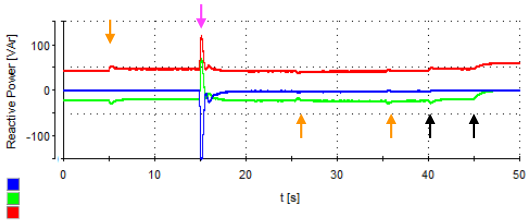

(d) Reactive power provided by the inverters to the load.

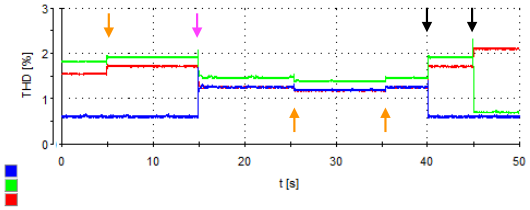

(e) Total harmonic distortion.

Figure 12: Voltage regulation at the PCCs with nonlinear load (Section 5.2.3). Red, green and blue lines are, respectively, for VSC 1, 2 and 3. Load change, plug-in and unplugging events are indicated with orange, magenta and black arrows, respectively.

5.3 Experimental results: plug-and-play and coordinated control

In this Section, we validate the combination of the coordinated control layer presented in Section 4 and PnP primary regulators.

As a first test, we consider the same experimental scenario as in Section 5.2.3, complemented with the coordinated controllers presented in Section 4.1 for voltage tracking at the PoL. This operation is desirable because, as shown in Figure 12a, PnP regulators alone fail to keep the PoL voltage at the nominal value, even though the voltages at the PCCs are stabilized. As highlighted in Section 4, this issue is due to the fixed voltage set-points for the PnP controllers. In this experiment, we activate coordinated controllers at time $t = 20$ s. Consequently, as shown in Figure 13a, the voltages at the PCCs increase in order to track the nominal PoL voltage. Moreover, the proposed coordinated controllers are capable to keep the PoL voltage at the desired level (by regulating the voltages at the PCCs) even when load changes (at times $t = 25$ s and $t = 35$ s) and disconnection of inverters (at $t = 40$ s and $t = 45$ s) are performed (see Figure 13). We also highlight that the presence of the coordinated controllers does not affect the frequency profiles (see Figure 13b). On the other hand, Figure 13d reveals that the total reactive power is still not shared equally between the inverters.

Parameter	Symbol	Value	Units
Virtual impedance			
Virtual resistance	$R_{i,v}$	3	Ω
Virtual inductance	$L_{i,v}$	0.03	H
Voltage tracking at the PoL			
Module proportional term	K_{PV}	10^{-3}	-
Module integral term	K_{IV}	0.6	-
Phase proportional term	$K_{P\phi}$	10^{-3}	-
Phase integral term	$K_{I\phi}$	4	-
Reactive power sharing			
Reactive power proportional term	K_{PQ}	10^{-4}	-
Reactive power integral term	K_{IQ}	10^{-2}	-
Electrical Setup			
PCC reference voltage	V_{ref}	230	V
ImG frequency	f_0	50	Hz
Switching frequency	f_{sw}	10	kHz
Filter resistance	R_{ti}	0.1	Ω
Filter inductance	L_{ti}	1.8	mH
Filter capacitance	C_{ti}	25	μF
Line resistance	R_i	0.1	Ω
Line inductance	L_i	1.8	mH
Phase resistive load	$R_{a,b,c}$	57-115-230-460	Ω
Nonlinear load	R_{NL}	460	Ω

Table 1: Electrical setup and control parameters.

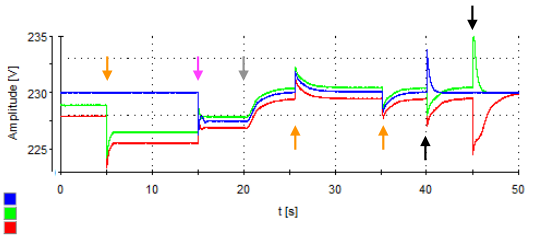

(a) Voltages V_i at the PCCs (phase a).

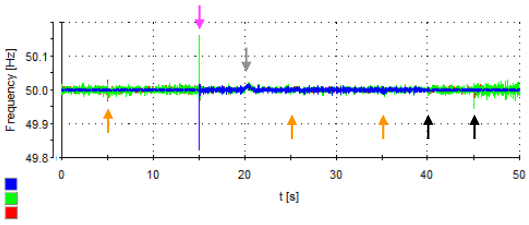

(b) Frequencies (phase a).

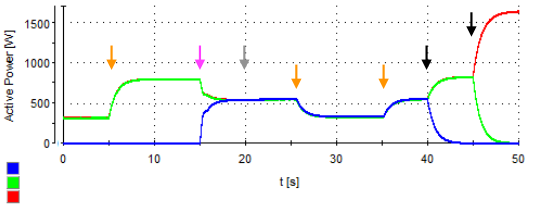

(c) Active power provided by the inverters to the load.

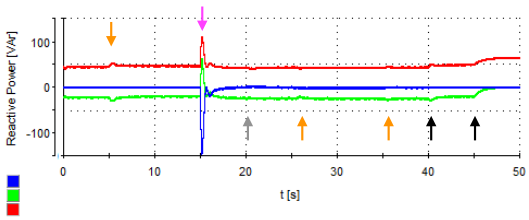

(d) Reactive power provided by the inverters to the load.

Figure 13: PnP regulators and coordinated controllers for voltage tracking at the PoL with nonlinear load. Red, green and blue lines are, respectively, for VSC 1, 2 and 3. Load change, plug-in and unplugging events are indicated with orange, magenta and black arrows, respectively. Moreover, the grey arrow denotes the activation of secondary controllers described in Section 4.1.

In order to ameliorate also aspect, we run a second experiment in which the previous control

scheme is complemented with coordinated controllers for reactive power sharing (described in Section 4.2). In particular, we notice that, right after their activation (at time $t = 20$ s), the total reactive power is equally shared (see Figure 14b, to be compared with Figure 13d). This goal is achieved through the computation of terms ΔV_i^Q in (17), which are shown in Figure 14a.

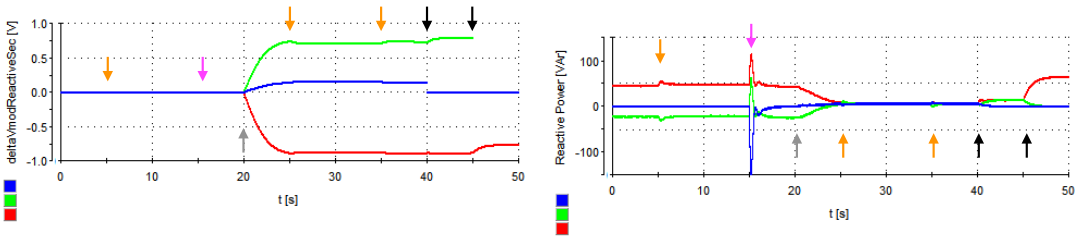

(a) Amplitude deviations ΔV_i^Q in (17) leading to the sharing of total reactive power.

(b) Reactive power produced by each VSC.

Figure 14: PnP regulators and coordinated controllers for voltage tracking at the PoL and reactive power sharing with nonlinear load. Red, green and blue lines are respectively for VSC 1, 2 and 3. Load change, plug-in and unplugging events are indicated with orange, magenta and black arrows, respectively. Moreover, the grey arrow denotes the simultaneous activation of secondary controllers described in Sections 4.1 and 4.2.

6 Conclusions

In this paper, we showed how to adapt the PnP control scheme [1, 10] for voltage and frequency regulation in AC ImGs to bus-connected topologies. Moreover, we introduced a secondary control layer and performed an experimental validation of the overall control hierarchy. Using the parallel connection of three VSCs, we showed that stability, efficient tracking of the voltage bus and sharing of reactive power can be obtained. Moreover, experiments with linear and nonlinear loads show that the harmonic distortion and imbalance ratio are kept within acceptable bounds. In our implementation, time-synchronization of DGU clocks and the secondary control layer assume all-to-all communication among DGUs. Future research will focus on distributing these computations as well, by exploiting only partial communication among DGUs and, as in [33], consensus-like protocols for estimating averages of global variables

7 Acknowledgment

The authors wish to thank Alessandro Floriduz for insightful discussions.

References

[1] S. Riverso, F. Sarzo, and G. Ferrari-Trecate, "Plug-and-play voltage and frequency control of islanded microgrids with meshed topology," *IEEE Trans. Smart Grid*, vol. 6, no. 3, pp. 1176–1184, 2015.

[2] D. Olivares, A. Mehrizi-Sani, A. Etemadi, C. Canizares, R. Iravani, M. Kazerani, A. Hajimiragha, O. Gomis-Bellmunt, M. Saeedifard, R. Palma-Behnke, G. Jimenez-Estevez, and N. Hatziargyriou, "Trends in microgrid control," *IEEE Trans. Smart Grid*, vol. 5, no. 4, pp. 1905–1919, 2014.

[3] J. M. Guerrero, M. Chandorkar, T. Lee, and P. C. Loh, "Advanced Control Architectures for Intelligent Microgrids — Part I: Decentralized and Hierarchical Control," *IEEE Transactions on Industrial Electronics*, vol. 60, no. 4, pp. 1254–1262, 2013.

[4] M. Ranaboldo, B. D. Lega, D. V. Ferrenbach, L. Ferrer-Martí, R. P. Moreno, and A. García-Villoria, "Renewable energy projects to electrify rural communities in cape verde," *Applied energy*, vol. 118, pp. 280–291, 2014.

[5] G. Kyriakarakos, A. I. Dounis, S. Rozakis, K. G. Arvanitis, and G. Papadakis, "Polygeneration microgrids: a viable solution in remote areas for supplying power, potable water and hydrogen as transportation fuel," *Applied Energy*, vol. 88, no. 12, pp. 4517–4526, 2011.

[6] J. Kumagai, "The rise of the personal power plant," *IEEE Spectr.*, vol. 6, no. 51, pp. 54–59, 2014.

[7] A. H. Etemadi, E. J. Davison, and R. Iravani, "A Decentralized Robust Control Strategy for Multi-DER Microgrids - Part I: Fundamental Concepts," *IEEE Trans. Power Del.*, vol. 27, no. 4, pp. 1843–1853, 2012.

[8] M. Babazadeh and H. Karimi, "A Robust Two-Degree-of-Freedom Control Strategy for an Islanded Microgrid," *IEEE Trans. Power Del.*, vol. 28, no. 3, pp. 1339–1347, 2013.

[9] C. D. Persis, N. Monshizadeh, J. Schiffer, and F. Dörfler, "A lyapunov approach to control of microgrids with a network-preserved differential-algebraic model," in *2016 IEEE 55th Conference on Decision and Control (CDC)*, Dec 2016, pp. 2595–2600.

[10] S. Riverso, F. Sarzo, and G. Ferrari-Trecate, "Plug-and-play voltage and frequency control of islanded microgrids with meshed topology," Tech. Rep., 2014. [Online]. Available: http://arxiv.org/abs/1405.2421

[11] S. Riverso, M. Farina, and G. Ferrari-Trecate, "Plug-and-Play Decentralized Model Predictive Control for Linear Systems," *IEEE Trans. Autom. Control*, vol. 58, no. 10, pp. 2608–2614, 2013.

[12] S. Riverso, "Distributed and plug-and-play control for constrained systems," Ph.D. dissertation, Università degli studi di Pavia, 2014.

[13] K. De Brabandere, B. Bolsens, J. Van den Keybus, A. Woyte, J. Driesen, and R. Belmans, "A voltage and frequency droop control method for parallel inverters," *IEEE Trans. Power Electron.*, vol. 22, no. 4, pp. 1107–1115, 2007.

[14] J. Kim, J. M. Guerrero, P. Rodriguez, R. Teodorescu, and K. Nam, "Mode adaptive droop control with virtual output impedances for an inverter-based flexible AC microgrid," *IEEE Trans. Power Electron.*, vol. 26, no. 3, pp. 689–701, 2011.

[15] V. Venkatasubramanian, H. Schattler, and J. Zaborszky, "Fast Time-Varying Phasor Analysis in the Balanced Three-Phase Large Electric Power System," *IEEE Trans. Autom. Control*, vol. 40, no. 11, pp. 1975–1982, 1995.

[16] M. Tucci, A. Floriduz, S. Riverso, and G. Ferrari-Trecate, "Plug-and-play control of AC islanded microgrids with general topology," in *European Control Conference (ECC)*, 2016, pp. 1493–1500.

[17] F. Dörfler and F. Bullo, "Kron reduction of graphs with applications to electrical networks," *IEEE Transactions on Circuits and Systems I: Regular Papers*, vol. 60, no. 1, pp. 150–163, 2013.

[18] G. Kron, *Tensor analysis of networks*. John Wiley and Sons, 1939.

[19] J. Schiffer, C. A. Hans, T. Kral, R. Ortega, and J. Raisch, "Modelling, analysis and experimental validation of clock drift effects in low-inertia power systems," *IEEE Transactions on Industrial Electronics*, 2016.

[20] H. Han, X. Hou, J. Yang, J. Wu, M. Su, and J. M. Guerrero, "Review of power sharing control strategies for islanding operation of AC microgrids," *IEEE Transactions on Smart Grid*, vol. 7, no. 1, pp. 200–215, Jan 2016.

[21] J. C. Vasquez, J. M. Guerrero, M. Savaghebi, J. Eloy-Garcia, and R. Teodorescu, "Modeling, Analysis, and Design of Stationary-Reference-Frame Droop-Controlled Parallel Three-Phase Voltage Source Inverters," *IEEE Trans. Ind. Electron.*, vol. 60, no. 4, pp. 1271–1280, 2013.

[22] R. H. Park, "Two-Reaction Theory of Synchronous Machines - Generalized Method of Analysis - Part I," *Transactions of the American Institute of Electrical Engineers*, vol. 48, no. 3, pp. 716–727, 1929.

[23] J. He and Y. Lee, "Analysis and design of interfacing inverter output virtual impedance in a low voltage microgrid," in *IEEE Energy Conversion Congress and Exposition (ECCE)*, Atlanta, GA, USA, September 12-16, 2010, p. 2857–2864.

[24] A. Phadkeand, J. Thorp, and M. Pai, *Synchronized Phasor Measurements and Their Applications*. New York, NY, USA: Springer, 2008.

[25] J. Vig, "Quartz crystal resonators and oscillators for frequency control and timing applications: A tutorial," U.S. Army Communications-Electronics Command, Fort Monmouth, NJ, USA, Tech. Rep. Tech. Rep. SLCET-TR-88-1 (Rev. 8.4.2), 2009.

[26] R. Gusella and S. Zatt, "The accuracy of the clock synchronization achieved by tempo in berkeley unix 4.3 bsd," *IEEE Trans. Softw. Eng.*, vol. 15, no. 7, pp. 847–853, 1989.

[27] "IEEE Draft Standard Profile for Use of IEEE 1588 Precision Time Protocol in Power System Applications," *IEEE PC37.238/D21.3, January 2017*, pp. 1–40, Jan 2017.

[28] Q. Shafiee, J. M. Guerrero, and J. C. Vasquez, "Distributed Secondary Control for Islanded Microgrids — A Novel Approach," *IEEE Trans. Power Electron.*, vol. 29, no. 2, pp. 1018–1031, 2014.

[29] F. Bullo, *Lectures on Network Systems*. Version 0.85, 2016. [Online]. Available: http://motion.me.ucsb.edu/book-lns

[30] A. Yazdani and R. Iravani, *Voltage-Sourced Converters in Power Systems: Modeling, Control, and Applications*. Hoboken, New Jersey, USA: John Wiley & Sons, 2010.

[31] R. Teodorescu, M. Liserre, and P. Rodriguez, *Grid converters for photovoltaic and wind power systems*. Chichester, West Sussex, UK: John Wiley & Sons, 2011.

[32] IEEE, "IEEE Recommended Practice for Monitoring Electric Power Quality," IEEE Std 1159$^{\text{TM}}$-2009, 3 Park Avenue, New York, NY 10016-5997, USA, Tech. Rep. June, 2009.

[33] Q. Shafiee, C. Stefanovic, T. Dragicevic, P. Popovski, J. Vasquez, and J. Guerrero, "Robust networked control scheme for distributed secondary control of islanded microgrids," *IEEE Trans. Ind. Electron.*, vol. 61, no. 10, pp. 5363–5374, 2014.